PERMAFROST AND PERIGLACIAL PROCESSES
Permafrost and Periglac. Process. **17**: 341–355 (2006)
Published online in Wiley InterScience
(www.interscience.wiley.com) DOI: 10.1002/ppp.566

Profiles of Temporal Thaw Depths beneath Two Arctic Stream Types using Ground-penetrating Radar

Troy R. Brosten, [1]* *John H. Bradford,* [1] *James P. McNamara,* [1] *Jay P. Zarnetske,* [2] *Michael N. Gooseff* [3] *and W. Breck Bowden* [4]

[1] Department of Geosciences, Boise State University, Boise, ID, USA
[2] Department of Aquatic, Watershed, & Earth Resources, Utah State University, Logan, UT, USA
[3] Department of Geology & Geological Engineering, Colorado School of Mines, Golden, CO, USA
[4] Rubenstein School of the Environment and Natural Resources, University of Vermont, Burlington, VT, USA

ABSTRACT

Thaw depths beneath arctic streams may have significant impact on the seasonal development of hyporheic zone hydraulics. To investigate thaw progression over the 2004 summer season we acquired a series of ground-penetrating radar (GPR) profiles at five sites from May–September, using 100, 200 and 400 MHz antennas. We selected sites with the objective of including stream reaches that span a range of geomorphologic conditions on Alaska's North Slope. Thaw depths interpreted from GPR data were constrained by both recorded subsurface temperature profiles and by pressing a metal probe through the active layer to the point of refusal. We found that low-energy stream environments react much more slowly to seasonal solar input and maintain thaw thicknesses longer throughout the late season whereas thaw depths increase rapidly within high-energy streams at the beginning of the season and decrease over the late season period. Copyright © 2006 John Wiley & Sons, Ltd.

KEY WORDS: ground-penetrating radar; permafrost; thaw bulb; arctic streams

INTRODUCTION

Streams on the North Slope of Alaska can be broadly classified as peat or alluvial. This streambed condition can be considered a geomorphologic property of the stream. Several studies have shown that stream geomorphology can have strong controls on hyporheic flow paths (Harvey and Bencala, 1993; Morrice *et al.*, 1997; Wroblicky *et al.*, 1998; Kasahara and Wondzell, 2003). In streams underlain by permafrost, hyporheic flow is the movement of water from the channel into the active layer and back. For the purpose of this paper the thaw bulb is defined as the active layer area directly beneath streambed channels, whereas more common usage defines it as the thawed zone under or surrounding a man-made structure placed on or in permafrost (Frozen Ground Data Center, 2005). Thus, hyporheic flow carries heat into the bed sediments and as a result controls the depth of thaw, setting up a feedback loop between stream geomorphology, hyporheic flow and depth of thaw. To understand how streambed morphologies control thaw bulb expansion, which in turn affects hyporheic processes, it is important to understand the temporal evolution of the thaw bulb in streams with differing morphologies.

Arcone *et al.* (1992, 1998a) successfully illustrated ground-penetrating radar (GPR) capabilities to profile

* Correspondence to: Troy R. Brosten, Department of Geosciences, Boise State University, 1910 University Drive, Boise, ID 83725, USA.
E-mail: troybrosten@mail.boisestate.edu

Contract/grant sponsor: US National Science Foundation; contract/grant number: OPP 03-27440.
Contract/grant sponsor: Department of Geosciences, Boise State University.

Received 23 February 2006
Revised 13 September 2006
Accepted 15 September 2006

groundwater and taliks beneath frozen stream channels on the Sagavanirktok flood plain. Bradford *et al.* (2005) showed that it is possible to measure the depth of thaw under peat-bed streams across open water in August 2003 using GPR. These studies were limited in scope in that they provided either early season measurements within a frozen alluvial steam environment or one measurement in time within a peat-bed stream. The purpose of the current study is to provide a time series of the evolution of the thaw bulb under peat-bed and alluvial stream types beneath open water during the summer season. This directly supports ongoing studies by the authors to investigate hyporheic dynamics in arctic streams (Zarnetske *et al.*, in press).

FIELD SITES

The Kuparuk watershed is underlain by continuous permafrost with thicknesses ranging from 250 m near the foothills to over 600 m near the coast (Osterkamp and Payne, 1981). Temperatures at 150 cm deep range between -9°C to 3°C, averaging -1°C annually at locations where the active layer thaws to depths of over 150 cm. Annual air temperatures range from -40°C to 21°C and averaged -8°C for 2004 (Arc LTER Weather Data, 2004).

Study sites, located in the Kuparuk watershed (Figure 1), were selected to include stream reaches that spanned a range of geomorphologic conditions in rivers and streams on Alaska's North Slope. The streams were divided into two categories: (1) low-energy water flow with organic material lining the streambeds (peat streams) and (2) high-energy water flow with cobble to gravel material lining the streambeds (alluvial streams).

The Peat Inlet (PI) and Green Cabin (GC) sites represent the low-energy water flow environment and are described as beaded streams (deep pools connected by shallow, narrow channels). The GC stream reach is the stream right channel entering a confluence located upstream of Green Cabin Lake and is characterised by two large pools connected by a shallow channel. The upstream pool has a peat-lined stream bottom while the downstream pool is gravel-lined along the streambed. Radar profiles were collected across the middle of both pools and across the connecting channels upstream and downstream of each pool. To represent results at this site and avoid redundancy, only two of the five profile lines will be discussed (Table 1).

The PI stream reach flows into Toolik Lake and is characterised by large, deep pools (12 m wide, 2.5 m deep) connected by relatively deep channels. Radar profiles were collected across one of the deeply incised connecting channels in the same location where Bradford *et al.* (2005) collected radar profiles in August 2004 (Table 1).

I-8 stream is in close proximity to the PI site and also flows into Toolik Lake. It, however, represents the high-energy flow environment. The I-8 Inlet site represents a run section of the stream and (8I) is located upstream of I-8 Lake. The next site, I-8 Outlet (8O), is located downstream of I-8 Lake, where radar profiles were acquired across a pool and riffle section of the stream (Table 1).

Oksrukuyik Creek (OC), located just upstream of the Dalton Highway crossing, is a hybrid of the two previous categories. The stream reach is described as beaded and is characterised by a series of large incised pools connected by relatively fast moving, shallow channels. However, the streambed bottom along the entire reach is lined with gravel-to-cobble sized rocks, rather than organic matter, which indicates intermittent high-energy flow events. Radar profiles were gathered across one of the pools and across the upstream and downstream connectors of the same pool. Results from this site will focus on the images collected over the pool (Table 1).

METHODS

GPR data were collected at the five sites from May–September 2004. Profiles were gathered on a weekly to monthly basis to measure changes in the thaw bulb thickness over the summer season and to evaluate the effectiveness of GPR within the varying environments. In addition, we recorded channel and thaw bulb temperatures using thermocouples placed at various substream depths within two of the five GPR data collection sites (PI and 8I) to help constrain and verify GPR interpretations.

GPR

GPR is a non-invasive method used to explore the shallow subsurface with electromagnetic waves. The transmitting antenna creates a pulsed electric field which propagates into the subsurface and is reflected where abrupt changes in electrical properties occur across interfaces. The receiving antenna records a trace of the reflected wave field in time. Multiple measurements are made along the surface, producing a cross-sectional reflection profile image of electric

DOI: 10.1002/ppp

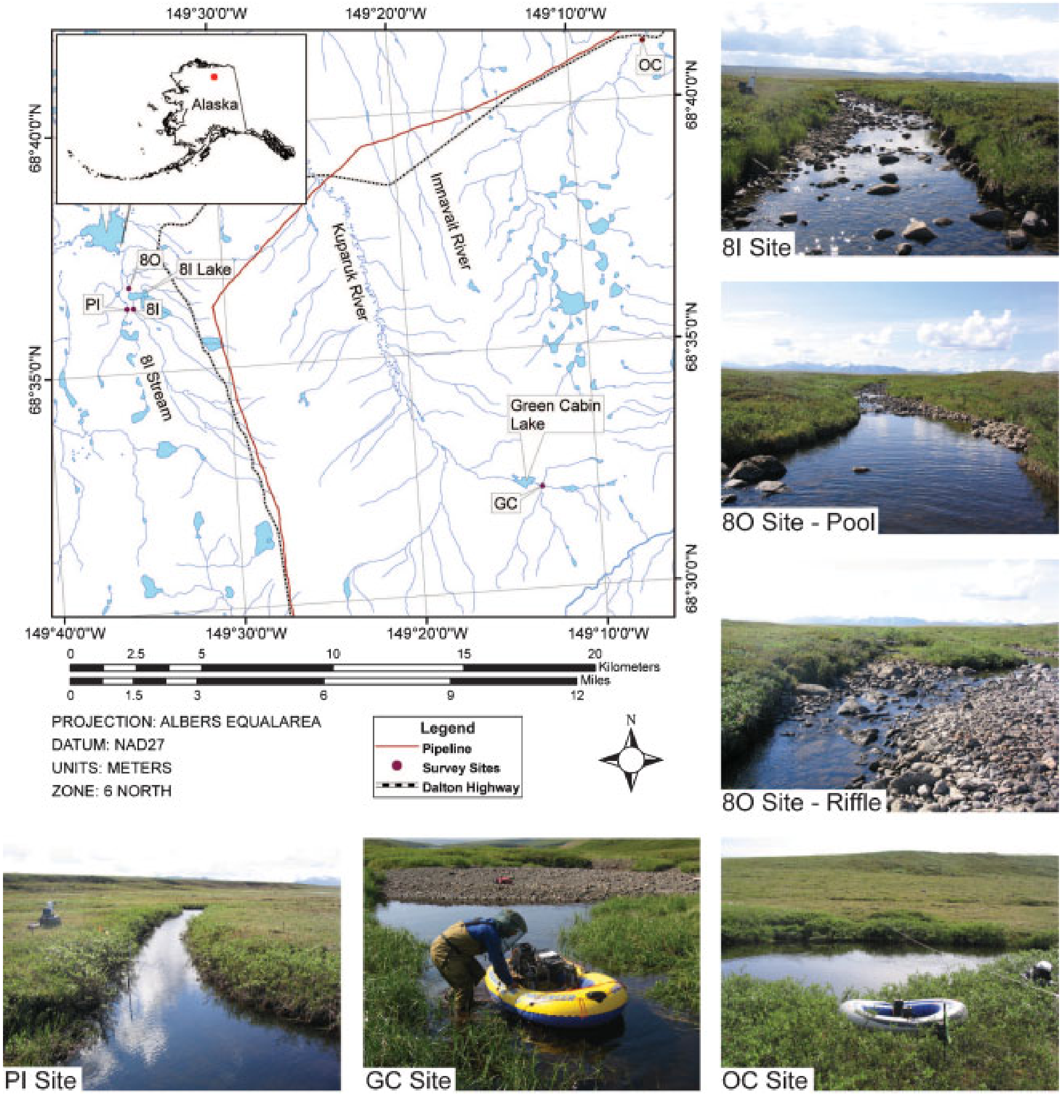

Figure 1 Locations of the five study sites within the Kuparuk watershed. This figure is available in colour online at www.interscience.wiley.com/journal/ppp.

impedance contrasts in the subsurface (Davis and Annan, 1989).

There is a large electrical contrast between water and ice. Using the time dependence equation given by Olhoeft (1981) the dielectric constant for water, at 0°C, is 87–88 and 3.2 for ice (Davis and Annan, 1989). Consequently, as water freezes within the subsurface, the dielectric permittivity (a measure of molecular polarisability of the wet sediments) decreases while the velocity of propagation increases (Scott *et al.*, 1990). Because GPR reflections primarily result from contrasts in electrical permittivity, GPR is an ideal tool for mapping the boundary between saturated soils and permafrost. Numerous studies have successfully used GPR to detect spatial and temporal variations in the permafrost boundaries within terrestrial soils (Wong *et al.*, 1977; Pilon *et al.*, 1985; Doolittle *et al.*, 1990, 1992; Arcone *et al.*, 1998b; Hinkel *et al.*, 2001).

Problems that arise when collecting substream radar images include attenuation of signal due to the strong frequency dependence of radar wave velocity and

DOI: 10.1002/ppp

Table 1 Site names with stream morphology and GPR profile descriptions.

	Site Name	Geomorphology/GPS Coord.	GPR Profile Description
High energy	8I Inlet (8I)	Gravel to cobble-lined stream with riffle-pool-riffle morphology 0.97% gradient 06 W 0394707, 7612535	Run 5 m across and 0.2 m deep Subsurface temperature sensors installed near profile lines
	8I Outlet (8O)	Gravel to cobble-lined stream with riffle-pool-riffle morphology 1.18% gradient Pool-06W 0394582, 7613443 Riffle-06W 0394593, 7613456	Pool-5 m across and 0.6 m deep Riffle-4 m across and 0.2 m deep
Low energy	Green Cabin (GC)	Organic-lined with beaded morphology. Channel walls have a gradual gradient where the connectors are very shallow with fast moving water. Pool section streambed bottom is lined with cobble material. Connector-06W 0409402, 7603959 Pool-06W 0409390, 7603956	Connector-2 m across and 0.2 m deep Pool-8 m across and 1 m deep
	Peat Inlet (PI)	Organic-lined stream with beaded morphology. Deeply incised pools and connectors with near-vertical channel walls. 0.90% gradient 06W 0394444, 761294	Connector-2 m across and 1 m deep Subsurface temperature sensors installed near profile line
High/low energy	Okruknyik Creek (OC)	Organic-lined stream with beaded morphology. Streambed bottom lined with gravel/cobble material indicating high-energy events 0.16% gradient 06W 0414902, 7620835	Pool-12 m across and 2 m deep

image distortion due to velocity contrasts. High frequencies travel faster and attenuate more quickly in water, which causes the dominant frequency to shift towards the lower end of the spectrum, resulting in lower resolution potential. For the data presented here, frequency decreases due to loading and frequency-dependent attenuation are significant and measurable such that attenuation through water lowers the frequency in 200 and 100 MHz data to ~120 and ~70 MHz, respectively (Bradford *et al.*, 2005). Stream water discharge and temperature variations can increase the dissolved solid concentration levels in the water, which cause higher conductivities and result in greater attenuation rates and even lower resolution potential (Bradford *et al.*, 2005). Water conductivity values at the study sites were very low (~40 μS/cm), with no apparent seasonal variation, so their effects on the data are negligible. Additionally, image distortion occurs where reflections are pushed down due to large velocity contrasts between water and saturated soils. Depth migration with the right velocities corrects for the distortion by placing the reflectors in their proper spatial location. Despite these limitations, several studies have successfully demonstrated high-resolution water bottom images over cold-region freshwater bodies (Delaney *et al.*, 1990; Arcone *et al.*, 1992, 1998a; Schwamborn *et al.*, 2002; Best *et al.*, 2005).

GPR resolution is limited by wavelength λ which is related to velocity, v, and frequency, f, through the relation $\lambda = v/f$. This relationship shows that higher frequencies result in smaller wavelengths which are capable of resolving finer features. However, higher frequencies also attenuate more quickly, therefore decreasing the depth of investigation; thus a tradeoff exists between depth of investigation and resolution potential. For this study, the wavelength relationship to velocity works in our favour because the velocity within the water-saturated thaw bulb region is lower than in the permafrost region, leading to greater resolution potential within the area of interest.

Data were acquired using a Sensors and Software PE100A pulsed radar system with a high-power transmitter (1000 V) used for all antenna frequencies. Early in the field season we used the 400 and 200 MHz antennas to maximise resolution potential, and then shifted to the 200 and 100 MHz antennas later in the summer to increase the depth of penetration. We placed the radar antennas in the bottom of a small rubber boat, then pulled the boat across the bank and through the stream while collecting radar traces at a constant distance interval via a string odometer

DOI: 10.1002/ppp

system. Stakes were placed at the start and end points of the profiles so that the GPR lines were collected at the same locations throughout the season. Despite the location control, differences are apparent in some of the stream profiles due to variations in stream water discharge.

In addition, depth to the thaw front (freeze/thaw interface) was measured on the stream banks and shallow streambed areas by pressing a metal probe into the ground to the point of refusal. At 8I and PI, subsurface temperature profiles were used to constrain GPR interpretations with the assumption that the depth at which the temperature is 0°C is the boundary between thawed and frozen layers.

We applied the following processing flow to each dataset:

1 Time zero correction with first break correlation to remove start of record delay and system drift.
2 DC shift and bandpass filtering with a 25–50–400–800 (for the 200 MHz) and a 12–25–200–400 (for the 100 MHz) Ormsby filter to attenuate the low frequency transient and high frequency random noise.
3 Amplitude correction which varied by site.
4 Kirchhoff depth migration coupled with iterative velocity model refinement (Yilmaz, 2001).

Because we were interested in thaw bulb depths, our velocity models only included values for water and the water-saturated substrate material. A velocity value of 0.032 m ns^{-1} was used for water at 0°C, and a velocity value of 0.05 m ns^{-1} was used for saturated peat material based on results reported by Bradford *et al.* (2005) and in other studies (Moorman *et al.*, 2003; Davis and Annan, 1989). From the migration velocity analysis (using a velocity value of 0.07 m ns^{-1} for the saturated gravel/sand material) we collapsed the diffractions and minimised migration artefacts.

High-amplitude water-bottom and permafrost multiples, and diffraction patterns caused by out-of-plane point sources within the gravel-lined stream site profiles presented interpretation challenges. Time lapse images helped identify the thaw front despite the presence of multiples or diffraction patterns. Additionally, due to radar resolution limitations, temperature data profiles significantly improved our ability to interpret the thaw plane in early season radar images.

Temperature Measurement

Temperatures were measured using Type-T thermocouple wire connected to a Campbell Scientific CR10X datalogger and AM16/32 multiplexer using a CR107 reference thermistor. Errors associated with Type-T thermocouples are ± 1.0°C over the range of −65 to 130°C. Thermocouples were installed in vertical profiles by driving a steel sleeve and interior bar into the streambed. The bar was then removed and the thermocouples were inserted into the sleeve. Lastly, the sleeve was removed from the sediment and pulled over the thermocouple wire, leaving the thermocouples in place. We installed four streambed profiles and one soil profile in 8I and two streambed profiles in PI at 20 cm increments to varying depths. Temperature profiles at site 8I reached a depth of 107 cm, while those at site PI reached a depth of 38 cm. The shallow depths at PI are due to frozen soil and deep water at the time of installation. Continuous subsurface temperature readings were recorded from late May throughout the remaining year.

RESULTS

Low Energy

At the GC site (connector), the late-May reflections (200 MHz) of the thaw front were difficult to distinguish from the water-bottom reflections due to resolution limitations where $\lambda/4$ provides an approximate vertical resolution limit (Yilmaz, 2001). Assuming a dominant frequency of 200 MHz with loading at ~120 MHz and a velocity in water-saturated peat of 0.05 m ns^{-1}, the signal wavelength is 0.416 m and the vertical resolution limits are roughly 10 cm, meaning that objects separated by less than this distance cannot be individually identified. For the 100 MHz antennas with loading at ~70 MHz and a velocity of 0.07 m ns^{-1} in water-saturated gravel the vertical resolution is 25 cm. Within a month the boundary became discernible (Figure 2a and 2b). As the thaw depth increased we recorded a separate and easily recognisable strong, continuous reflection from the thaw front where the maximum thaw bulb thickness, 51 cm, was recorded on 21 September (Figure 2c and 2d). The later season profiles show relatively weak reflections at the water-to-peat bottom boundary due to relatively small contrasts in the permittivity between the two media. Also notable is the pulldown in the reflectors under the channel due to the lateral velocity change from the water-filled channel to water-saturated soil (Figure 2a and 2c) and correct positioning of the reflector pullup after depth migration was applied (Figure 2b and 2d).

Resolution was not problematic in early-season, 200 MHz profiles from the pool site (GC pool) due to initially deeper thaw depths where the thaw bulb was

DOI: 10.1002/ppp

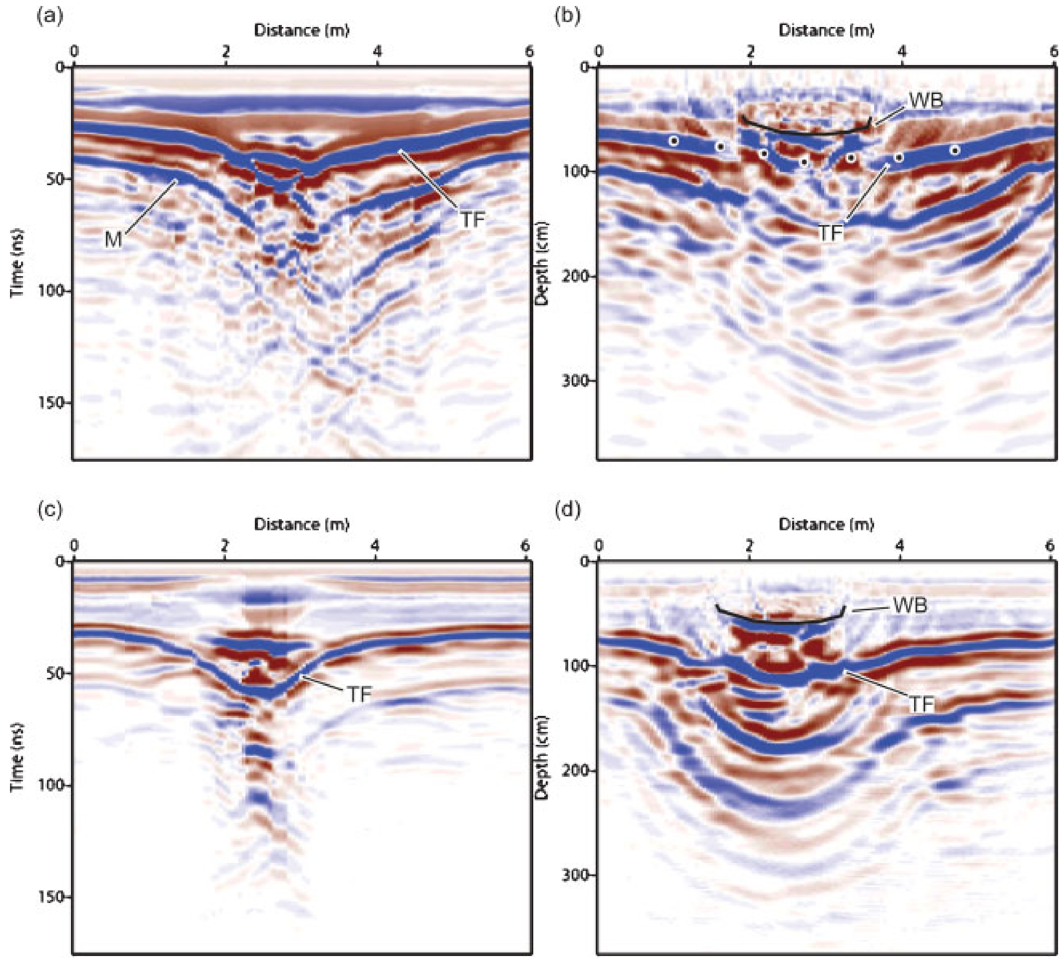

Figure 2 (a) Preprocessed image from GC connector recorded on 28 June 2004 (200 MHz), (b) depth migrated image, (c) preprocessed image recorded 21 September 2004 (200 MHz), (d) depth migrated image. (—) Interpreted water bottom, (•) thaw front, (TF) thaw front reflection, (WB) water bottom, (M) multiple. This figure is available in colour online at www.interscience.wiley.com/journal/ppp.

easily resolved (Figure 3a and 3b). The maximum thaw bulb thickness, 104 cm, was recorded on 21 September (Figure 3c and 3d). Relative reflection strength was higher in pool profiles in comparison to connector profiles. This difference in amplitude indicates greater permittivity contrast caused by the gravel-lined pool bottom.

Results at the PI site were very similar to those noted within the GC-connector profiles. The thaw front proved easy to identify from a strong continuous reflection throughout the season (Figure 4). Despite the physical differences, the PI site being deeply incised with greater water depths, the thaw depth seasonal patterns at PI and GC connector are remarkably similar.

Subsurface temperature values recorded by the thermocouples helped us to interpret the thaw front in the early season profiles and confirmed interpretations in the later season images. We began logging temperature profiles on 31 May. Prior to our initial logging, profile A (see Figure 4) had thawed to 18 cm, but profile B did not thaw to 16 cm until 9 days later (12 June). Likewise, profile A thawed to 38 cm on 27 June while profile B remained frozen at 36 cm until 11 July. Warmer temperature values recorded at profile A correlate with the radar profiles where a deeper reflection is noted on the right side of the streambed (Figure 4 b), indicating greater thaw depths beneath the thalweg of the stream. Maximum thaw beneath the thalweg may be caused

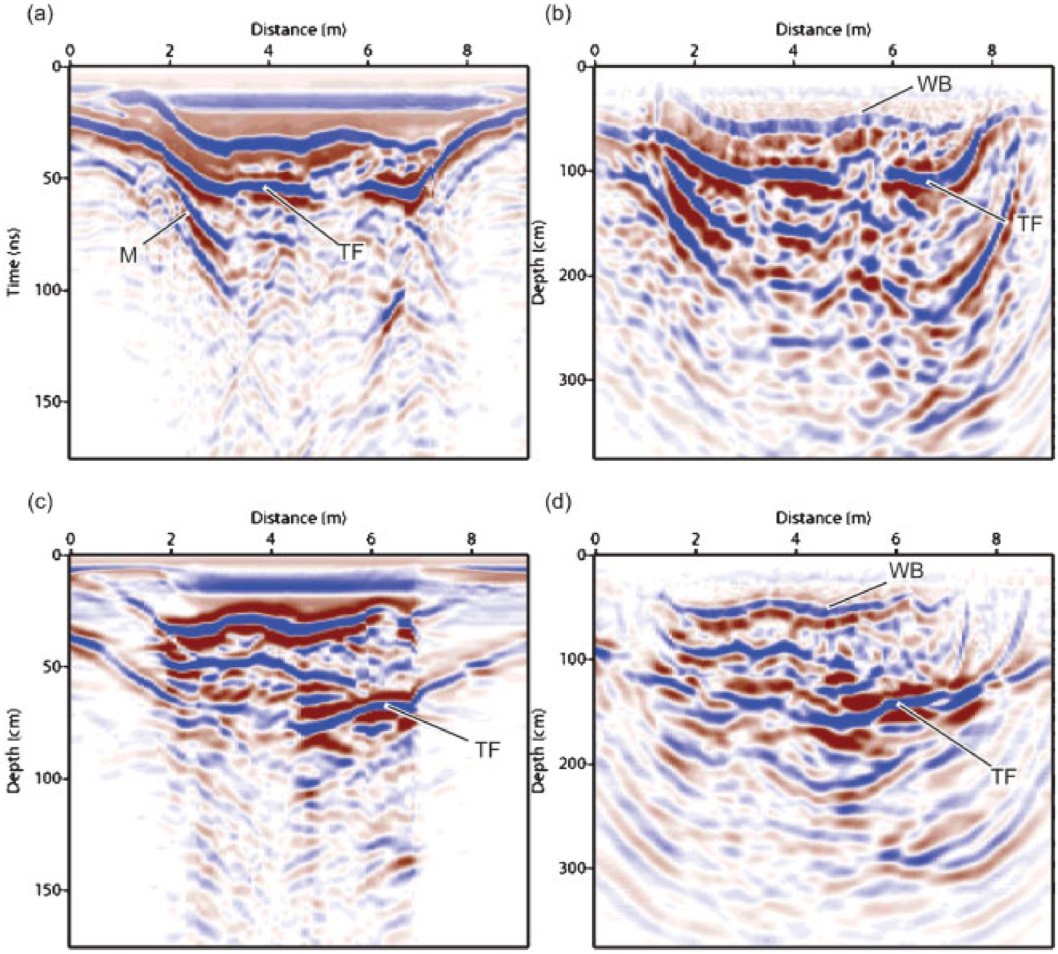

Figure 3 (a) Preprocessed image from GC pool recorded on 28 June 2004 (200 MHz), (b) depth migrated image, (c) preprocessed image recorded 21 September 2004 (200 MHz), (d) depth migrated image. (TF) Thaw front reflection, (WB) water bottom. (M) multiple. This figure is available in colour online at www.interscience.wiley.com/journal/ppp.

by more heat going into the system from the warmer instream water temperatures. As the season advances and the temperatures increase, thalweg effects become less prevalent and the maximum thaw depth is more evenly distributed across the centre of the streambed (Figure 4d). The August profile from PI (Figure 4a and 4b) also correlates with the radar image collected by Bradford *et al.* (2005) where the maximum thaw depth was estimated at 61 cm in August 2003 and 63 cm in August 2004.

The alluvial-peat OC reach, despite having a peat-influenced morphology, experienced the greatest overall thaw depths compared to the other peat-lined stream sites. We collected early season radar images with 200 MHz antennas and then shifted to 100 MHz antennas in the later season as the depth of investigation increased. In the early season profile, within the unmigrated image, there is a continuous thaw front reflection obscured by high-amplitude water bottom diffractions (Figure 5a). After migration, the diffractions are collapsed and the water bottom and frost table reflectors move to their correct spatial locations, resulting in a distinct reflection at the thaw front (Figure 5b). The August radar image, collected with 100 MHz antennas, captured a distinct reflection of the thaw front at a depth of 233 cm. The boundary then becomes partly obscured from multiple scattering

DOI: 10.1002/ppp

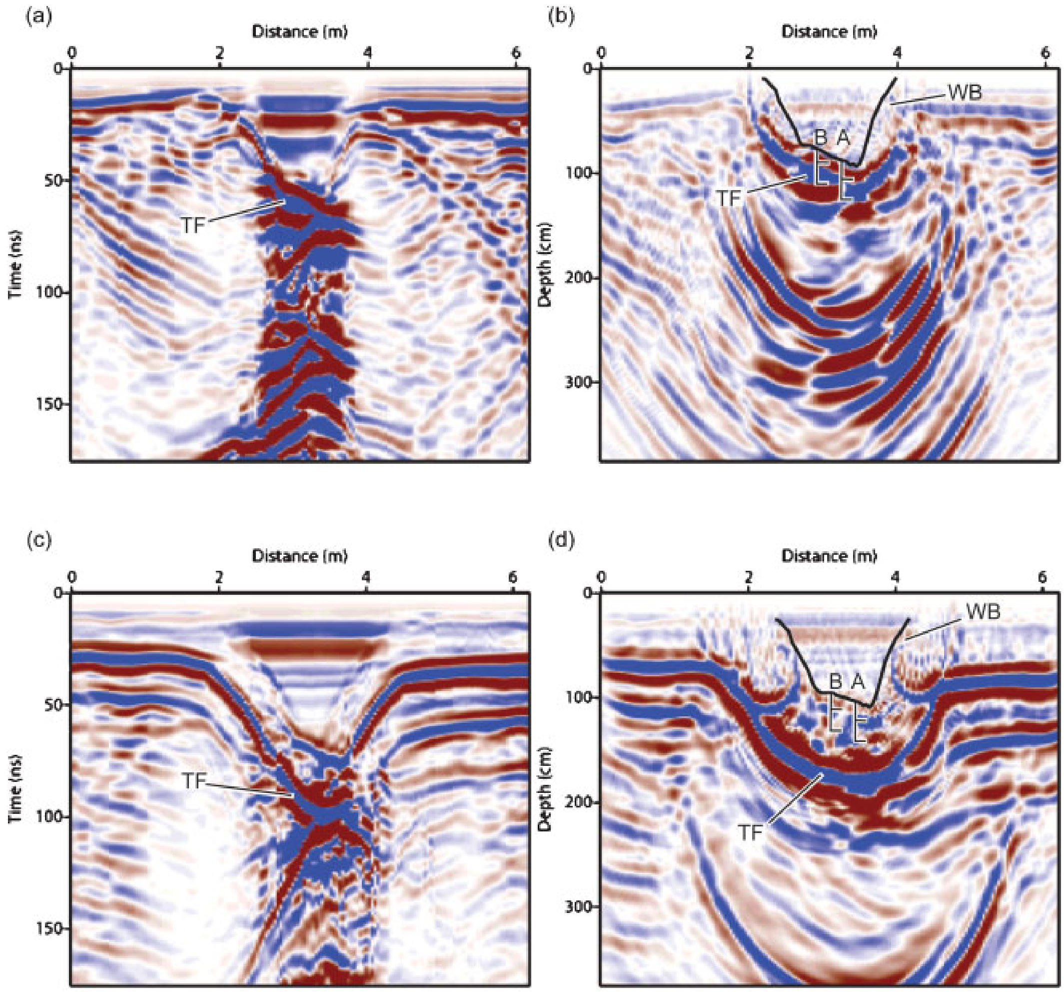

Figure 4 (a) Preprocessed image from PI site recorded on 7 June 2004 (200 Mhz), (b) depth migrated image (temperature sensor locations represented at B (16 and 36 cm) and A (18 and 38 cm)), (c) preprocessed image recorded on 6 August 2004 (200 MHz), (d) depth migrated image. (—) Interpreted water bottom, (TF) thaw front reflection, (WB) water bottom. This figure is available in colour online at www.interscience.wiley.com/journal/ppp.

and water bottom multiples as the boundary depths decrease towards the sides of the channel (Figure 5c). The thaw front in the migrated image of the same profile is difficult to distinguish due to over-migration of multiples (Figure 5d). Migration algorithms only account for primary travel times, so multiples are not treated correctly and always appear over-migrated.

High Energy

Imaging the thaw bulb within the gravel-lined stream sites proved to be difficult due to the highly heterogeneous environment. Variable sand-to-gravel-to-cobble-to-boulder sized material under the streambeds caused, in some cases, severe multiple scattering patterns within the radar images. These diffraction patterns effectively masked the location of the frost table beneath the streambed channels. Despite these limitations we were able to interpret the thaw front from a number of images.

Radar images collected at the 8I site were among the most difficult to interpret, but subsurface temperature data collected at this site confirmed early-season depth-to-thaw boundaries. Some of the later season profiles resolved the thaw front relatively

DOI: 10.1002/ppp

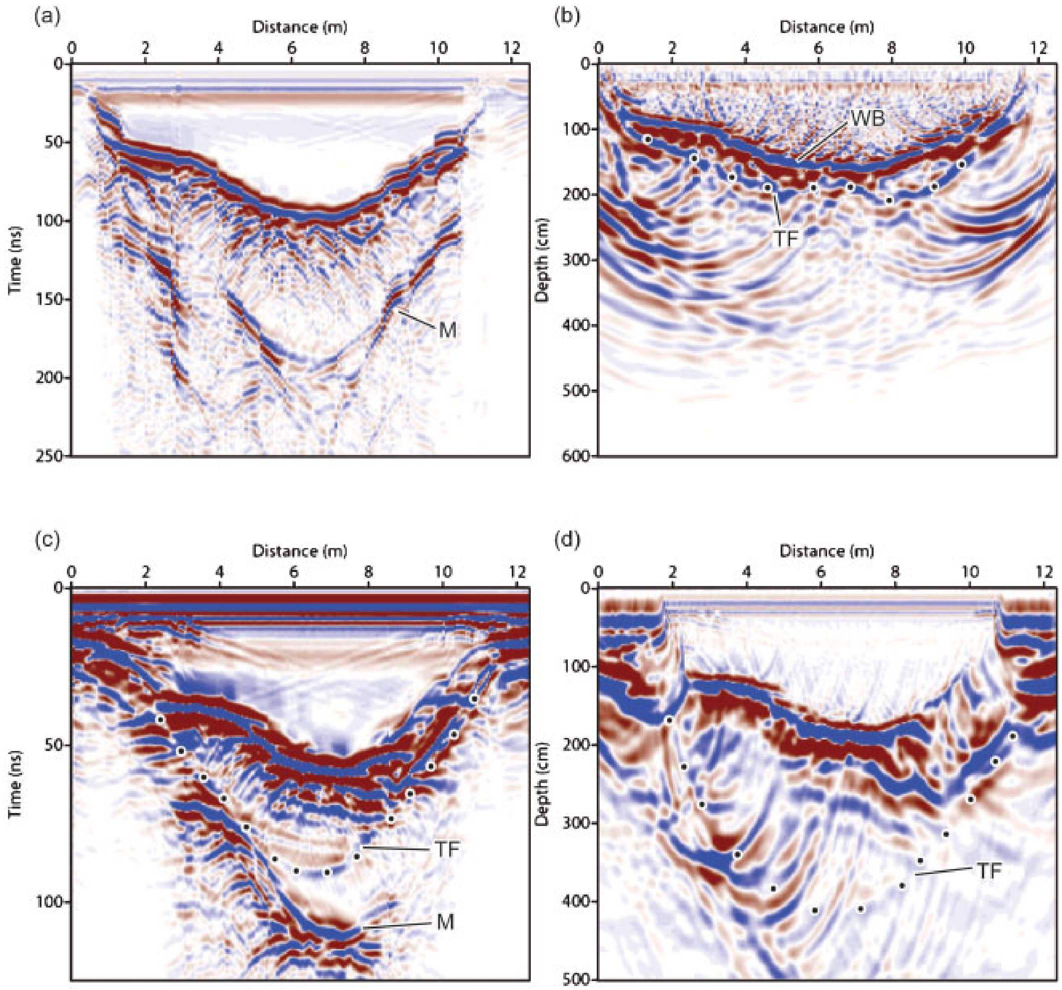

Figure 5 (a) Preprocessed image from OC recorded on 2 June 2004 (200 MHz), (b) depth migrated image, (c) preprocessed image recorded 5 August 2004 (100 MHz), (d) depth migrated image. (•) Thaw front, (TF) thaw front reflection, (WB) water bottom, (M) multiple. This figure is available in colour online at www.interscience.wiley.com/journal/ppp.

well, whereas after migration the same images became difficult to interpret. This was due to two-dimensional (2D) limitations where three-dimensional point source diffractions cannot be collapsed by 2D migration to their correct spatial location because they occur off the 2D GPR line.

Stream temperature logging began at 8I following the snowmelt period on 31 May 2004. Three thermocouple profiles in the streambed show that subsurface thaw had started prior to 31 May. In profile A the streambed was thawed past 47 cm, but remained frozen at greater depths. The streambed thawed to 67, 87 and 107 cm on 2 June, 5 June and 7 June, respectively. In profiles B and C the streambed was thawed past 80 and 82 cm, respectively, prior to our arrival in late May, but appears to have thawed to 100 cm and 102 cm on 2 June. Thaw occurs in the adjacent soil later than in the streambed. The soil was slightly above 0°C at 8 cm deep when we began logging, but did not thaw until 14 June and 19 June at 28 and 48 cm, respectively.

Following thaw, all four streambed temperature profiles behaved similarly with peak temperatures occurring in early July. Streambed temperatures rose and fell, mimicking air temperature with slight lags at depth. Throughout the season subsurface temperature values decreased with depth until late August when temperatures at greater depths became warmer than

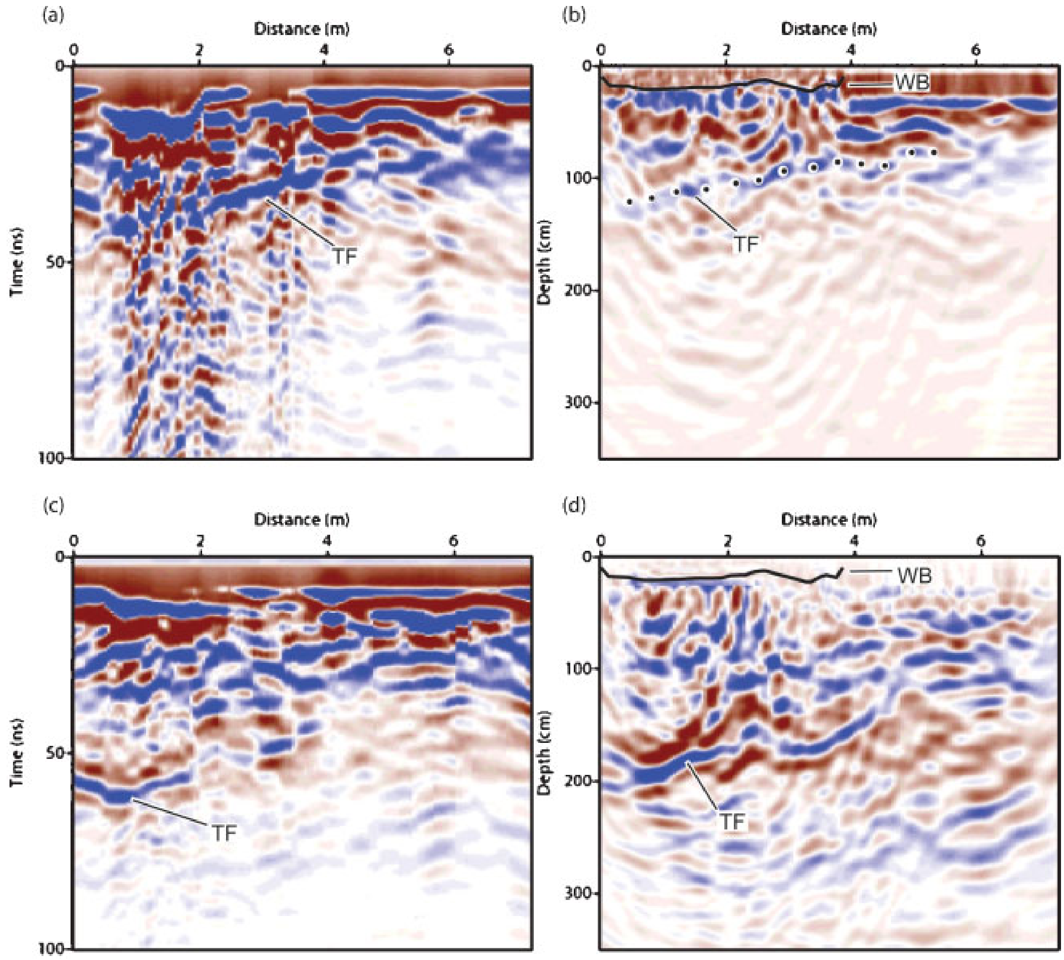

Figure 6 (a) Preprocessed image from 8O riffle recorded on 7 June 2004 (200 MHz), (b) depth migrated image, (c) preprocessed image recorded 22 June 2004 (200 MHz), (d) depth migrated image. (—) Interpreted water bottom, (•) thaw front, (TF) thaw front reflection, (WB) water bottom. This figure is available in colour online at www.interscience.wiley.com/journal/ppp.

temperatures at shallower depths. All profiles and all depths reached 0°C by late September.

Images collected at the pool and riffle sections at the 8O site were more easily interpreted than the 8I profiles, probably because the subsurface was more homogeneous. Radar profiles over the pool illustrate a strong continuous reflection from the thaw front throughout the season. Radar images over the riffle showed a clear reflection from the thaw front in both the migrated and unmigrated images (Figure 6). Profiles over the riffle resolved a much deeper thaw front under the exposed gravel bar, left side, and a thinner thawed region under the active stream section (0–4 m). Overall interpreted maximum thaw depths were greater at the 8O-riffle site than at the 8I site.

DISCUSSION AND CONCLUSIONS

Our results demonstrate that GPR methods are useful in monitoring subsurface seasonal thaw within both peat and alluvial stream environments. In some of the early-season profiles the thaw front within the peat-lined streams was difficult to identify, due to resolution limitations. Later season images were successful due to a typically homogeneous subsurface, small contrast between peat and water, and smooth

DOI: 10.1002/ppp

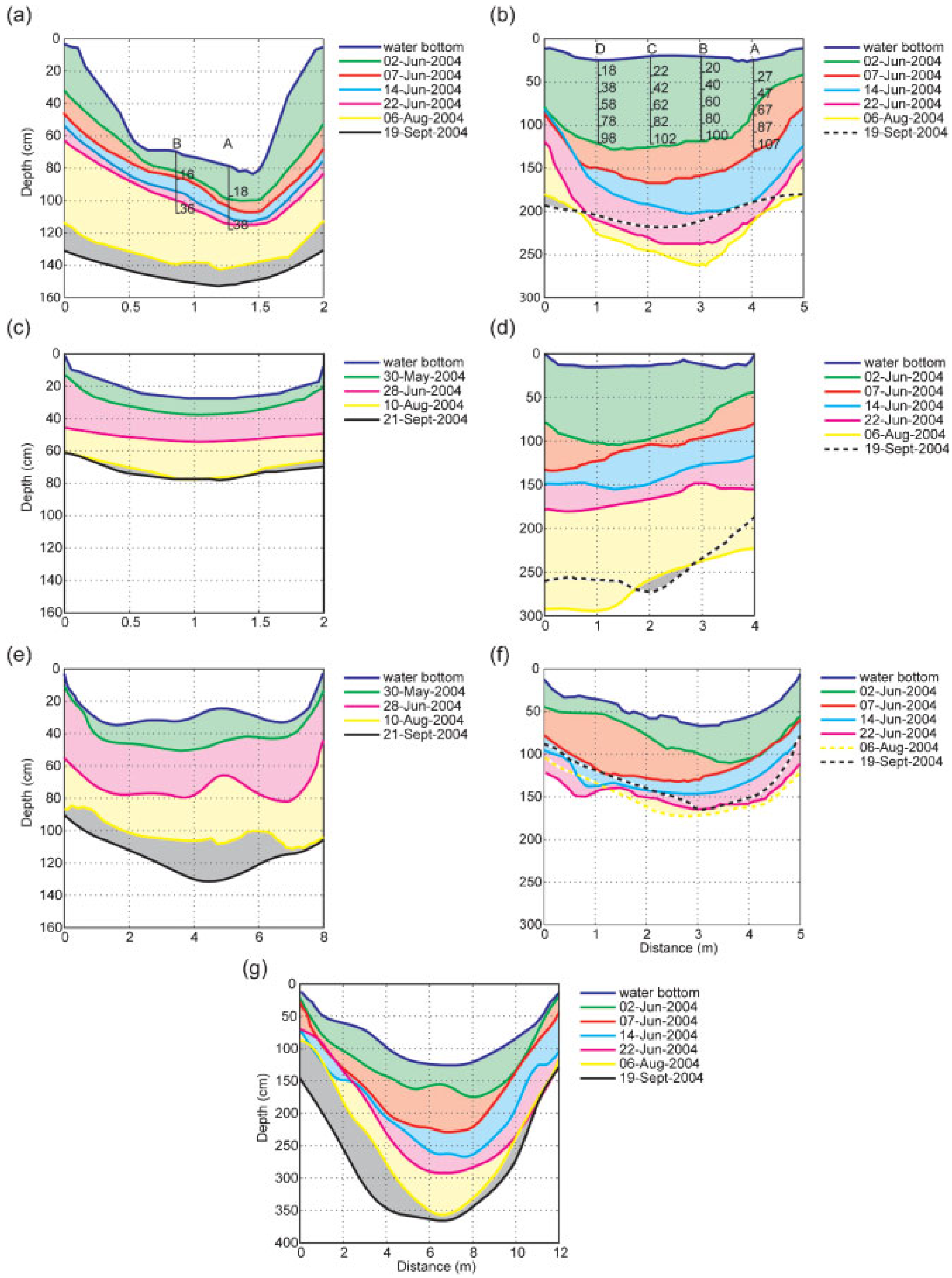

Figure 7 Frost/thaw boundary depths interpreted from GPR images and temperature data when available. The axes scales vary between some of the subfigures in order to display interpretation details for each site. (- - -) Frost/thaw boundary interpreted at a shallower depth than earlier GPR profiles. (a) PI with temperature sensor locations (cm) measured from the stream channel bottom, (b) 8I with temperature sensor locations (cm) measured from the stream channel bottom, (c) GC connector, (d) 8O riffle, (e) GC pool, (f) 8O pool, (g) OC.

DOI: 10.1002/ppp

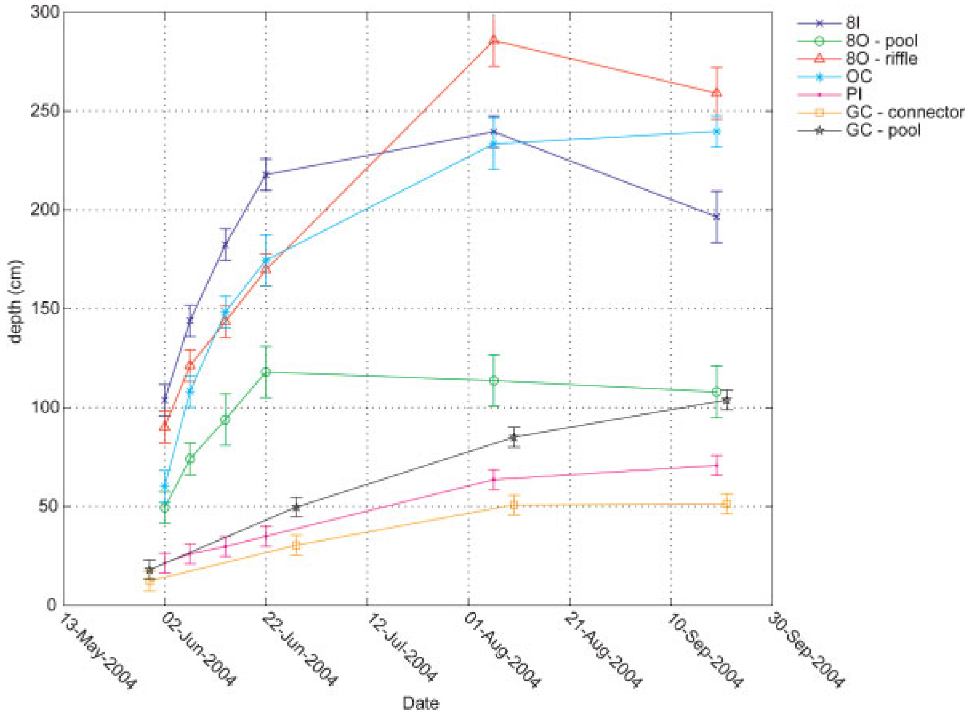

Figure 8 Maximum thaw bulb depths for the five sites. For the 200 MHz data a ± 5 cm error is calculated for the peat-lined stream sites. At the gravel-lined stream site a ± 8 cm error is estimated for interpretations made from the 200 MHz data and a ± 13 cm error is estimated for the 100 MHz data. This figure is available in colour online at www.interscience.wiley.com/journal/ppp.

channel bottoms. Successful images within gravel-lined streams were strongly site dependent and interpretations were significantly more complicated due to diffraction patterns caused by a highly heterogeneous subsurface and the irregular water/streambed interface. Identification of the thaw front reflection within the gravel-lined streams was greatly improved by gathering time-lapse profiles over the summer season where the moving boundary was properly identified. The same reflection in a one-time seasonal image could be misinterpreted as a multiple.

Thaw bulb development within the two stream environments was distinctly different. Figure 7 illustrates interpretations of the thaw front depths for each site, from GPR and temperature data, throughout the field season period. Thaw depths increased to greater than 1 m within the first 4 weeks of the season within gravel-lined streams and to only 32 cm within peat-lined streams (Figures 7 and 8). Based on multiple images gathered over the season, maximum thaw depths within the gravel-lined streams, which may represent the permafrost table, were recorded in August. In September the gravel-lined sites began to refreeze while the peat-lined sites continued to thaw. Maximum thaw depths in the latter were recorded up to the last site visit in September, indicating a heat lag in the peat-lined streams (Figure 8).

Temperature profiles recorded at 8I coincide with the interpreted GPR profiles for the period when the thaw bulb grew rapidly in the early season. Thermocouples did not reach to the depth of the interpreted permafrost table recorded in August. However, the temperature gradient which inverted in late August (cooler temperatures at shallow depths) indicates a change in the thermal input into the system (Figure 9). The September GPR interpretation illustrates thaw bulb retreat from colder temperatures (Figure 7).

Early season thaw depths between 8I and 8O riffle were similar in trend but much greater thaw depths were interpreted at the 8O riffle in the later season. Variation in the thaw bulb thicknesses between 8I and the 8O riffle is likely due to heat transfer from a greater surface area of exposed rocks (left side) within the riffle section at 8O. Overall thaw depths within the 8O pool section were much smaller and are likely due to

DOI: 10.1002/ppp

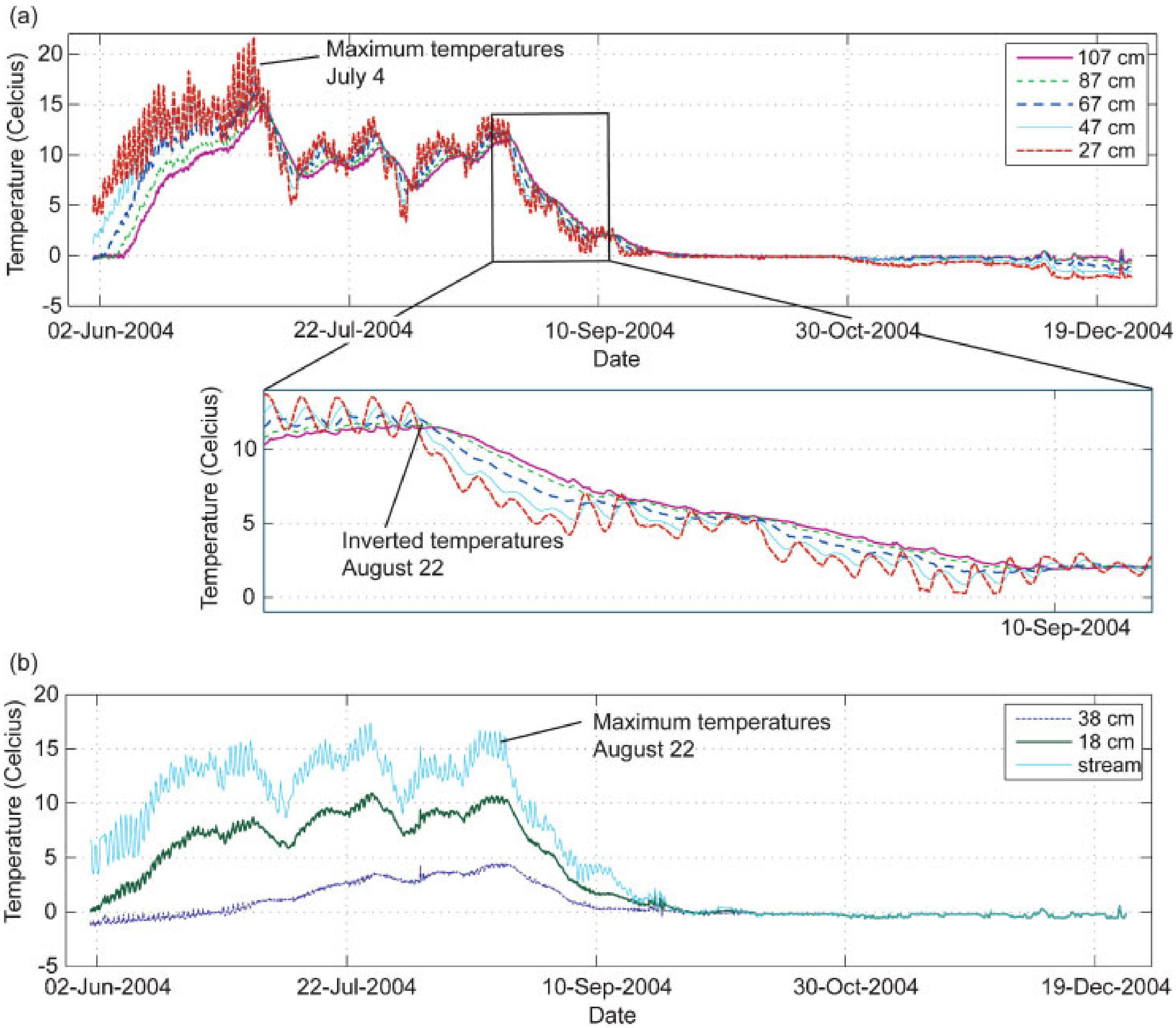

Figure 9 Temperature data from (a) string A at 8I site and (b) string A at PI site. This figure is available in colour online at www.interscience.wiley.com/journal/ppp.

minimal rock exposure compared with the 8I and 8O riffle sections.

Comparisons between temperature values recorded at PI and 8I illustrate distinct differences in thermal input between the two systems. Maximum temperatures were reached by 4 July and 22 August at 8I and PI, respectively. At the PI site, temperature gradients were much larger and shallow temperatures (16 and 18 cm) were always warmer than the deeper (36 and 38 cm) temperatures over the field season period. At 8I, temperature gradients were much smaller over a greater depth range, and a temperature inversion occurred at the same time maximum temperatures were recorded at 38 cm beneath the PI site (Figure 8). Differences between sites could be due to the deeper water at PI, combined with the peat lining that covers the streambed.

The pool profile at OC responded similarly to the pool section at GC in that thaw depths at both sites continued to increase up to the last site visit in September. However, the OC site recorded much greater thaw depths reaching a maximum of 240 cm on 20 September (Figure 8). One possible cause for the continued thaw at OC may be the result of more substantial and persistent flows experienced by OC which, in turn, promoted sub-channel thaw through September.

DOI: 10.1002/ppp

Comparisons between the two stream types illustrate distinct differences in seasonal thaw bulb development. Gravel-lined streams respond much more quickly to thermal input and peat-lined sites display a much slower response in early season and either maintain or expand their thawed regions through the late season (Figure 8). These observations indicate rapid heat absorption and heat loss in the gravel-lined streams whereas the peat-lined streams illustrate an insulating effect that extends past the time of maximum solar input.

ACKNOWLEDGEMENTS

We are grateful to K. Hill, R. Payn and M. Johnston for field assistance, and to the Arctic LTER program, Toolik Field Station camp personnel, VECO Polar Resources and Air Logistics for assistance with field logistics. We also thank Dr Steven Arcone, an anonymous reviewer and Dr Antoni Lewkowicz, Editor of *Permafrost and Periglacial Processes*, for their insightful comments, which substantially improved the manuscript. The US National Science Foundation funded this work under grant no. OPP 03-27440 with additional funding provided by the Department of Geosciences, Boise State University. The opinions, findings and conclusions or recommendations expressed in this material are those of the authors and do not necessarily reflect the views of the National Science Foundation.

REFERENCES

Arc LTER Weather Data. 2004. Toolik Lake Main. [online]. Available: http://ecosystems.mbl.edu/arc/data_doc/weather/tl/index.html [15 March 2006].

Arcone SA, Chacho EF, Delaney AJ. 1992. Short-pulse radar detection of groundwater in the Sagavanirktok River floodplain in early spring. *Water Resources Research* **28**: 2925–2936. DOI: 10.1029/92WR01308

Arcone SA, Chacho EF, Delaney AJ. 1998a. Seasonal structure of taliks beneath arctic streams determined with ground-penetrating radar. In *7th International Permafrost Conference Proceedings*, Lewkowicz AG, Allard M (eds). Centre d'études Nordiques, Université Laval: Sainte-Foy. Collection Nordicana **57**, 19–24.

Arcone SA, Lawson DE, Delaney AJ, Strasser JC, Strasser JD. 1998b. Ground-penetrating radar reflection profiling of groundwater and bedrock in an area of discontinuous permafrost. *Geophysics* **63**: 1573–1584. DOI: 10.1190/1.1444454

Best H, McNamara JP, Liberty L. 2005. Association of ice and river channel morphology determined using ground-penetrating radar in the Kuparuk River. *Arctic, Antarctic, and Alpine Research* **37**: 157–162.

Bradford JH, McNamara JP, Bowden W, Gooseff MN. 2005. Measuring thaw depth beneath peat-lined arctic streams using ground-penetrating radar. *Hydrological Processes* **19**: 2689–2699. DOI: 10.1002/hyp.5781

Davis JL, Annan AP. 1989. Ground-penetrating radar for high-resolution mapping of soil and rock stratigraphy. *Geophysical Prospecting* **37**: 531–551.

Delaney AJ, Arcone SA, Chacho , Jr EF. 1990. Winter short-pulse radar studies on the Tanana River, Alaska. *Arctic* **43**: 244–250.

Doolittle JA, Hardisky MA, Gross MF. 1990. A ground-penetrating radar study of active layer thicknesses in areas of moist sedge and wet sedge tundra near Bethel, Alaska, U.S.A. *Arctic and Alpine Research* **22**: 175–182.

Doolittle JA, Hardisky MA, Black S. 1992. A ground-penetrating radar study of Goodream Palsen, Newfoundland, Canada. *Arctic and Alpine Research* **21**: 336–339.

Frozen Ground Data Center. 2005. *Multi-language Glossary of Permafrost and Related Ground-ice Terms*, van Everdingen R (ed.) [online]. National Snow and Ice Data Center/World Data Center for Glaciology: Boulder, CO. Available: http://nsidc.org/fgdc/glossary/definitions.pdf [10 April 2006].

Harvey JW, Bencala KE. 1993. The effect of streambed topography on surface-subsurface water exchange in mountain catchments. *Water Resources Research* **29**: 89–98. DOI: 10.1029/92WR01960

Hinkel KM, Doolittle JA, Bockheim JG, Nelson FE, Paetozold R, Kimble JM, Traves R. 2001. Detection of subsurface permafrost features with ground-penetrating radar, Barrow, Alaska. *Permafrost and Periglacial Processes* **12**: 179–190. DOI: 10.1002/ppp.369

Kasahara T, Wondzell SM. 2003. Geomorphic controls on hyporheic exchange flow in mountain streams. *Water Resources Research* **39**: 3–14. DOI: 10.1029/2002WR001386

Moorman BJ, Robinson SD, Burgess MM. 2003. Imaging periglacial conditions with ground-penetrating radar. *Permafrost and Periglacial Processes* **14**: 319–327. DOI: 10.1002/ppp.463

Morrice JA, Valett HM, Dahm CN, Campana ME. 1997. Alluvial characteristics, groundwater-surface water exchange and hydrological retention in headwater streams. *Hydrological Processes* **11**: 253–269.

Olhoeft GR. 1981. Electrical properties of rocks. In *Physical Properties of Rocks and Minerals*, Touloukian YS, Judd WR, Roy RF (eds). McGraw-Hill: New York; 257–330.

Osterkamp TE, Payne MW. 1981. Estimates of permafrost thickness from well logs in northern Alaska. *Cold Regions Science and Technology* **5**: 13–27.

Pilon JA, Annan AP, Davis JL. 1985. Monitoring permafrost ground conditions with ground probing radar

(G.P.R.). In *Workshop on Permafrost Geophysics, Golden, Colarado*. US Army Corps of Engineers, Cold Regions Research and Engineering Laboratory, Hanover, New Hampshire, CRREL Special Report 85-5, 71–73.

Schwamborn GJ, Dix JK, Bull JM, Rachold V. 2002. High-resolution seismic and ground penetrating radar–geophysical profiling of a thermokarst lake in the western Lena delta, northern Siberia. *Permafrost and Periglacial Processes* **13**: 259–269. DOI: 10.1002/ppp.430

Scott WJ, Sellmann P, Hunter JA. 1990. Geophysics in the study of permafrost. In *Geotechnical and Environmental Geophysics, Vol. 1: Review and Tutorial*. Investigations in Geophysics 5, Society of Exploration Geophysicists: Tulsa, Oklahoma; 355–384.

Wong J, Rossiter JR, Olhoeft GR, Strangway DW. 1977. Permafrost: electrical properties of the active layer. *In situ. Canadian Journal of Earth Science* **14**: 582–586.

Wroblicky GJ, Campana ME, Valett HM, Dahm CN. 1998. Seasonal variation in surface-subsurface water exchange and lateral hyporheic area of two stream-aquifer systems. *Water Resources Research* **34**: 317–328. DOI: 10.1029/97WR03385

Yilmaz O. 2001. Seismic data analysis: processing, inversion, and interpretation of seismic data. Investigations in Geophysics 10, Society of Exploration Geophysicists: Tulsa, Oklahoma; 1000 pp.

Zarnetske JP, Gooseff MN, Brosten TR, Bradford JH, McNamara JP, Bowden WB. In press. Transient storage as a function of geomorphology, discharge, and permafrost active layer condition in arctic tundra streams. *Water Resources Research*.